Biophysical Reports

ARTICLE

Empirical asymmetric phonon sideband due to phonons in the protein matrix present in photosynthetic complexes: Time-domain response theory

Mohamad Toutounji[1,*]
[1]College of Science, Department of Chemistry, UAE University, Al-Ain, UAE

ABSTRACT The phonon spectral density plays a key role in probing the dynamical and spectral behavior of molecular aggregates. One may utilize the intimate connection between the one-phonon profile and the phonon spectral density to extract a plausible form of the spectral density of media with rich structure using advanced optical spectroscopy. The excitonic transition is normally accompanied by a broad, asymmetric phonon-side band due to the coupling to the phonons in the surrounding protein matrix present in photosynthetic complexes. The asymmetry in the one-phonon profile of a homogeneous absorption spectrum and other experiments performed on photosynthetic bacterial reaction centers (BRCs) led the Small group to employ a half-Gaussian distribution function on the red side and half-Lorentzian distribution function on the blue side of the absorption lineshape to account for the one-phonon profile asymmetrical shape and relaxation effects contributing to spectroscopy and dynamics of BRCs at hand. Different research groups successfully employed the theory of Small to simulate their photosynthetic spectral data so they could calculate the homogeneous absorption and hole-burned spectra of photosynthetic complexes. Although this report does not directly use the formulae of homogeneous absorption, hole-burning, and fluorescence line-narrowed spectra of BRCs, and photosynthetic complexes, developed by Hayes-Small, it builds on their idea of the phonon sideband asymmetric shape in deriving an accurate and computationally efficient linear electronic transition dipole moment time correlation function. Besides the compelling tractability and efficiency of this correlation function, it accounts for excitonic coupling and eliminates all the inconsistencies arising in the Hayes-Small theory.

WHY IT MATTERS Different research groups successfully employed the Hayes-Small theory (where a half-Gaussian function on the red side and half-Lorentzian distribution function on the blue side of the absorption spectrum is used to account for the one-phonon profile asymmetrical shape and relaxation effects) for photosynthetic complexes to simulate their photosynthetic spectral data to calculate absorption and hole-burned spectra in which the phonon sideband of the absorption and nonlinear optical experiments exhibit asymmetry. This work derives an accurate and computationally expedient dipole moment time correlation function for multimode systems. Besides the compelling tractability and efficiency featured by the correlation function discussed here, it accounts for asymmetric phonon profiles and excitonic coupling and eliminates all deficiencies and discrepancies arising in the Hayes-Small theory.

INTRODUCTION

Homogeneously broadened absorption spectra of condensed molecular systems in the low-temperature limit consist of a sharp peak called a zero-phonon line (ZPL), accompanied by a broad phonon sideband (PSB). Extensive research has been taking place to understand the dynamics of molecular aggregates, especially pigment-protein complexes (1–5). The shapes of linear homogeneous absorption spectra of condensed molecular systems reveal a wealth of structural and dynamical information about the nature of these systems. Further, the shape and breadth of spectral signals are affected by dephasing, relaxation, and dissipative factors, reflecting information about the identity of the molecular system at hand. These factors may be accounted for by employing the correct phonon spectral density, thereby leading to an accurate PSB, especially the one-phonon profile (fundamental

Submitted September 1, 2023, and accepted for publication January 25, 2024.

*Correspondence: mtoutounji@uaeu.ac.ae

Editor: Dmitrii Makarov.

https://doi.org/10.1016/j.bpr.2024.100146

transition) on which the subsequent multiphonon transitions (overtones) build (6–12). These overtones fold on the broadening of the fundamental transition (one-phonon profile) as shown by the MBO model (13), Toutounji et al. (11,14), and Hayes et al. (15). Their work (13–15) reports a formalism whereby the width folding of the overtones in the absorption spectra as the number of phonons associated with each transition, namely quantized damping. However, the work in Refs. (13,14) produces a *symmetric* one-phonon profile, namely Lorentzian distribution, since they assume Markovian and Condon dynamics. The one-phonon profile, which is an essential component of the PSB, is quite informative about the spectral density at work. Extracting the operative spectral density from a disordered system with rich structure, e.g., photosynthetic complexes, is a difficult task (6–10,15–19). Evidently, Debye spectral density does not seem to model the spectra in bacterial reaction centers (BRCs) and photosynthetic complexes (6–10,15–19).

The experiments performed on molecular chromophores embedded in proteins, polymers, and glasses have displayed *asymmetric* phonon profiles, (6–9,15–20) whereas theory, on the contrary, normally produces *symmetric* phonon profiles (vide supra). These symmetric profiles are Lorentzian distribution, resulting from Fourier transforming a simple time exponential decay that arise in Markovian, Condon, and harmonic dynamics. Small and co-workers employed hole-burning spectroscopy on chlorophylls embedded in the protein complex of *Rhodobacter sphaeroides* and *Rhodopseudomonas* (*Rps*.) *viridis* RCs to obtain detailed information on the linear electron-phonon coupling of protein phonons in antenna complexes that is defined by the Huang-Rhys factor S and the associated one-phonon profile. In these pigment-protein complexes, the one-phonon profile appears to be generally asymmetrically centered at 20–30 cm^{-1}. Small et al. (10,16,17) showed, guided by their experimental data, that a distribution function composed of a half-Lorentzian function on the high-energy side and a half-Gaussian function on the low-energy side in the frequency domain satisfactorily fits their spectra. Henceforth, the half-Gaussian distribution function on the red side and the half-Lorentzian distribution function on the blue side assignment of the spectrum will be referred to as a G-L distribution.

In light of the above, a G-L distribution was proposed to model the aforementioned asymmetric one-phonon profiles (15). Hayes-Small formalism (HSF) is frequency-domain based and has been utilized to carry out spectral and dynamical calculations, thereby interpreting experimental data successfully (6,10,15,16,21,22). To this end, experiments performed (6,9,10,15,16,21,22) on chlorophylls embedded in the protein complex showed that their spectra may satisfactorily fit to a G-L distribution in the frequency domain. In fact, Feng et al. (9) performed some calculations using parameters typically found in photosynthetic complexes and showed that employing G-L distribution to fit their spectral data was as gratifying as the lognormal distribution (19).

However, the corresponding electronic transition dipole moment time correlation function (or any time-dependent quantities that generate asymmetric PSB) of a photosynthetic dimeric complex using a G-L distribution function whereby both exciton-exciton coupling and exciton-phonon coupling are accounted for has not been reported. Although the exciton-exciton coupling will shift the vibronic bands, the exciton-phonon coupling will reflect the coupling strength of the matrix phonons to the excitonic transition, which, in our case, will lead to broad asymmetric PSB. (The electronic transition dipole moment time correlation function (EDMCF) may then be employed to calculate nonlinear optical signals to further probe pigment-protein complexes, as will be done in part II of this series using optical nonlinear response theory.) Although the phonon spectral density closely resembles the one-phonon profile of the PSB, we will present our new EDMCF in terms of the one-phonon profile exclusively, as part III will independently deal with more advanced spectral densities to probe linear and nonlinear signals in pigment-protein complexes and BRCs. Different environments have different phonon distributions, and learning about the nature of the distribution present in pigment-protein complexes may lead to better understanding of this protein vibrational structure, especially when probed using advanced spectroscopy techniques such as hole-burning, two-dimensional electronic spectra, and stimulated photon echo. As such, this would serve as an important biological implication of this work.

This work may be considered a first-time report of the linear electronic transition dipole moment correlation function in the time domain, whereby the broadening effects, PSB asymmetry, exciton-exciton coupling, and exciton-phonon coupling in BRCs are accounted for correctly. To this end, HSF suffers from discrepancies and deficiencies that are well elucidated by Jankowiak et al (10). Although the pigment-pigment interaction (excitonic coupling) treatment is missing in both HSF (15) and their corrected forms by Jankowiak et al. (10), the derived EDMCF herein accounts for these missing factors. Additionally, the computational expediency acquired by the derived EDMCF herein should be noted. Finally, having an EDMCF in the time domain, of which Fourier transform leads to *asymmetric* one-phonon profile, will allow a straightforward and expedient computation of

nonlinear optical signals, e.g., photon echo, pump-probe, hole-burning, and two-dimensional electronic spectra.

Despite the wide applicability, utility, and success of HSF in monomeric subunit FMO and weakly excitonically coupled photosynthetic complexes (6,18,21,23), the absence of the corresponding theory in the time domain has led to my writing this manuscript. More importantly, this work offers a remedy that eliminates critical deficiencies experienced by HSF in the frequency domain, especially for a multimode system (10). In summary, HSF 1) is mathematically intractable, hence computationally demanding, especially for multimode pigment-protein complexes; 2) experiences discrepancies and inconsistencies (in the case of systems with many modes and strong electron-phonon coupling, which is often the case in BRCs), as pointed out by Reppert(10); and 3) pigment-pigment coupling term, especially for a special pair BRC, is absent. Although Reppert et al. (10) have solved the discrepancies and inconsistencies experienced by HST, they made it more complex and less efficient computationally. As a point of fact, in the current form of their expression (10), besides more complexity, the expansion terms of the nested sums therein keep growing as the pigment-complex strength (Huang-Rhys factor, S) increases, especially at high temperatures. Also, no numerical strategy was reported for terminating these proportionally growing expansion terms, thereby causing accuracy issues to arise. As such, performing the direct inverse Fourier transform of HSF (or that of Reppert et al. (10)) analytically or numerically will only reproduce the same issues cited above. For this reason, it should be avoided. Additionally, HSF does not lead to any time-domain four-wave mixing signals, and the phonon profiles are reported using a conditional IF statement. Also, HSF was never derived but postulated. On the other hand, the work presented herein provides a derivation of a linear EDMCF with correct Franck-Condon factor (FCF), interpigment coupling, electronic dephasing, and asymmetric one-phonon profile shape. Although paper II (the second part of the series) will address the applicability of our work to nonlinear optical photon echo, pump-probe, and 2D electronic signals, part III will provide detailed spectral formalism of lognormal distribution function to linear and nonlinear temporal signals.

Theoretical setup for dimeric complexes

Consider an excitonically coupled dimeric system with nuclear vibrations coupled to a bath mode of harmonic oscillators. Assuming the identical monomers interacting through the dipole-dipole effect, the Hamiltonian of interest may be written as

$$H = \sum_{m=1}^{2} \varepsilon_m B_m^{\dagger} B_m + \sum_{mn} J_{mn}\, B_m^{\dagger} B_n + H_{vib} + H_{ex-vib} + H_{bath} + H_{ex-vib-bath} \tag{1}$$

where ε_m is the electronic transition energy of monomer (pigment) m, $B_m^{\dagger}$ is the electronic excitation Fermi creation operator, B_m is the electronic deexcitation Fermi annihilation operator, and J_{mn} is the Coulombic coupling between the electronic charge densities of the pigments making up the dimer (the Coulombic exchange interaction term has been dropped). The vibrational Hamiltonian reads

$$H_{vib} = \sum_{j} E_j b_j^{\dagger} b_j + 1/2, \tag{1a}$$

with E_j being the vibrational energy and $b_j^{\dagger}(b_j)$ the creation (annihilation) boson operators. Although the linear coupling exciton-vibrational Hamiltonian is

$$H_{ex-vib} = \sum_{jmn} m_j \omega_j^2 d_{jmn} B_m^{\dagger} B_n q_j, \tag{1b}$$

the bath Hamiltonian and the pigment-bath Hamiltonian $H_{ex-vib-bath}$ will be left unspecified for reasons that will become apparent later. The typical pigment-bath Hamiltonian in the literature reads

$$H_{ex-vib-bath} = \sum_{jmn} \upsilon_{jnm} B_m^{\dagger} B_n \left(b_j^{\dagger} + b_j \right), \tag{1c}$$

where υ_{jnm} is the pigment-bath coupling constant. Here q_j, m_j, ω_j, and d_{jmn} are coordinate, mass, frequency, and the upper linear displacement of vibrational mode j due to exciton-phono coupling, respectively. The dimer Hamiltonian may also be cast in the site basis set as

$$H = \sum_{m=1}^{2} \varepsilon_m |m\rangle\langle m| + \sum_{mn} J_{mn} |m\rangle\langle n| + \sum_{j} E_j |j\rangle\langle j| + \sum_{jmn} m_j \omega_j^2 d_{jmn}\, q_j |m\rangle\langle n| + H_{bath} + H_{ex-vib-bath} \tag{2}$$

It is noteworthy that the electronic Hamiltonian for monomer k may alternatively be written as

$$H_{el}(k) = H_{gk} |gk\rangle\langle ek| + H_{ek} |ek\rangle\langle gk| = H_{gk} B_k B_k^{\dagger} + H_{ek} B_k^{\dagger} B_k \tag{3}$$

Or simply written, for each monomer,

$$\boldsymbol{H_{el}} = \boldsymbol{H_g} |\boldsymbol{g}\rangle\langle \boldsymbol{g}| + \boldsymbol{H_e} |\boldsymbol{e}\rangle\langle \boldsymbol{e}| \tag{4}$$

to avoid clutter. By definition, $\boldsymbol{B_k} = |\boldsymbol{g}\rangle\langle\boldsymbol{e}|$ and $\boldsymbol{B_k^\dagger} = |\boldsymbol{e}\rangle\langle\boldsymbol{g}|$. Here $\boldsymbol{H_{gk}}$ and $\boldsymbol{H_{ek}}$ are the ground and excited states nuclear Hamiltonians for site/monomer k.

Assuming an electronic transition from a ground state $|\boldsymbol{g}\rangle$ to an excited state $|\boldsymbol{e}\rangle$, the resulting homogeneous absorption spectrum will have intensity, shape, and broadening, all of which are caused by the time evolution of the Hamiltonian in Eq. 1. The FCFs will give rise to the integrated intensity, whereas the absorption profile shape (e.g., Lorentzian, Gaussian, or Voigt), symmetry, and broadening are caused by the coupling to the bath and the associated dephasing processes, whereby the bath spectral density plays an essential role. Traditional treatment of dephasing processes through spin-boson coupling Hamiltonian would only result in *symmetric* Lorentzian or Gaussian profile (24,25). However, experiments performed on BRCs, show *asymmetric* absorption profile, half of which is Gaussian on the low-energy side and the other half is Lorentzian on the blue side of the spectrum. As such, although the bath form is left undetermined, its effects are accounted for as guided by experiments performed by Small et al. (15–17,21,22). The next section will derive the linear EDMCF, whereby the exciton-phonon coupling is accounted for that leads to overtones that fold themselves on the fundamental transition (one-phonon profile) that has an asymmetric shape made of half-Gaussian on the red side and half-Lorentzian on the high-energy side guided by Hayes-Small experimental findings (vide supra). The linear EDMCF is given by

$$\boldsymbol{F(t)} = \langle \boldsymbol{P(t)P(0)} \rangle \tag{5}$$

where the electronic polarization $\boldsymbol{P(t)} = \sum_{\boldsymbol{m}} \mu_{\boldsymbol{m}} (\boldsymbol{B_m^\dagger} + \boldsymbol{B_m})$ in which $\mu_{\boldsymbol{m}}$ is the dipole moment operator of monomer m. The linear EDMCF function in the Heisenberg representation reads

$$\boldsymbol{J(t)} = \boldsymbol{Tr}\left[\boldsymbol{e^{iHt/\hbar} P(0) e^{-iHt/\hbar} P(0)} \rho_{\boldsymbol{eq}}\right] \tag{6}$$

where the equilibrium density matrix is $\rho_{\boldsymbol{eq}}$ given by

$$\rho_{\boldsymbol{eq}} = \frac{\boldsymbol{e^{-\beta H}} |\boldsymbol{g}\rangle\langle\boldsymbol{g}|}{\boldsymbol{Z}} \tag{6a}$$

in which Z is the canonical partition function. The trace in Eq. 6 is taken over electronic, nuclear, and bath degrees of freedom. Although tracing over the electronic basis will project $\boldsymbol{F(t)}$ over in the nuclear and bath subspace, tracing over vibrations will give rise to FCFs, of a linearly coupled system, and tracing over the latter will lead to the spectral profile shape and the associated broadening.

For simplicity purposes, one may initially evaluate $\boldsymbol{F(t)}$ in the low-temperature limit for a vibrational mode j that yields, precluding broadening effects (homogeneous dephasing) and assuming no population transfer (24,25),

$$\boldsymbol{F_{jmn}(t)} = \boldsymbol{exp}\left[-\boldsymbol{i\varepsilon_{mn}t\delta_{mn}} - \boldsymbol{iJ_{nm}t} - \boldsymbol{S_{jnm}}\left(\boldsymbol{1} - \boldsymbol{R_{jnm}(t;\omega_j;\gamma_j)}\right)\right] \tag{7}$$

where $\boldsymbol{S_{jnm}}$ is the Huang-Rhys factor, which is responsible for linear exciton-phonon coupling strength; the reciprocal of γ_j signifies phonon dephasing time (damping constant); and $\boldsymbol{R_{jnm}(t;\omega_j;\gamma_j)}$ is the decoherence or nuclear dephasing function that arises due to the dimer-bath coupling. As part of evaluating $\boldsymbol{R_{jnm}(t;\omega_j;\gamma_j)}$, the asymptotic condition $\boldsymbol{R_{jnm}(t;\omega_j;\gamma_j)} \rightarrow \boldsymbol{e^{-i\omega_j t}}$ as $\gamma_j \rightarrow \boldsymbol{0}$ should be imposed to ensure the proper behavior of EDMCF. (Note that $\boldsymbol{R_{jnm}(t;\omega_j;\gamma_j)}$ affects only vibrational modes, which is why it is appended with the index j and has nil effect on the ZPL.) It is left unevaluated since the nature of the bath and its coupling to the dimer are yet unknown. Setting $\boldsymbol{R_{jnm}(t;\omega_j;\gamma_j)} = \boldsymbol{0}$ will give rise to a purely oscillatory correlation function in Eq. 7 and does not exhibit any damping or decoherence since bath effect has vanished ($\boldsymbol{R_{jnm}(t;\omega_j;\gamma_j)} = \boldsymbol{0}$). The ZPL profile has different symmetry, shape, and broadening than the transitions (vibronics) in the PSB; as such, the pure electronic and PSB regions undergo considerably different dephasing processes (13–22). To account for this spectral feature, the nuclear dephasing function $\boldsymbol{R_{jnm}(t;\omega_j;\gamma_j)}$ will initially be set to zero, only for now, so it only manifests itself in the PSB. However, the theory by HSF indicates that the ZPL adopts a Lorentzian profile, (13,14,26) leading to

$$\boldsymbol{F_{jnm}(t)} = \boldsymbol{exp}\left[-\boldsymbol{i\varepsilon_{mn}t\delta_{mn}} - \boldsymbol{iJ_{nm}t} - \boldsymbol{S_j}\left(\boldsymbol{1} - \boldsymbol{e^{-i\omega_j t}}\right) - \boldsymbol{\Gamma_{ZPL}|t|\,/\,2}\right] \tag{8}$$

Eq. 8 will render a ZPL width of $\Gamma_{\boldsymbol{ZPL}}$ and delta function (zero width) for all the subsequent phonon profiles (fundamental transition and overtones) on the blue side of the spectrum. Upon comparing Eqs. 7 and 8, their difference would reveal the impact of the nuclear dephasing function $\boldsymbol{R_{jnm}(t;\omega_j;\gamma_j)}$ on the optical lineshape. Now that we have secured the correct shape, symmetry, FCF, and width of the ZPL that is consistent with HSF finding (13,14,26), we next try to evaluate a plausible form of the nuclear dephasing function $\boldsymbol{R_{jnm}(t;\omega_j;\gamma_j)}$ that gives rise to an asymmetric broadening of the phonon profiles only.

One possible way to attempt modeling the effect of the bath on the system in the time domain is to look at the asymmetric shape of the one-phonon profile (fundamental transition) and its width first upon which the subsequent profiles build, thereby finding the form of $\boldsymbol{R_{jnm}(t;\omega_j;\gamma_j)}$. Accordingly, one may assume that the k-phonon profile (k ← 0 transition), which will be

denoted L_k, of the homogeneous absorption lineshape $I(\omega)$ of mode j with frequency ω_j may be postulated as

$$L_k \propto \left[u(\omega - k\,\omega_j) \frac{k/2\pi}{(\omega - k\omega_j)^2 + (k\gamma_j/2)^2} + \frac{1}{\sqrt{2\pi\sigma_j^2}} u(k\omega_j - \omega) e^{-(\omega - k\omega_j)^2 / 2\sigma_j^2} \right] \quad (9)$$

where $u(\omega)$ is the generalized unite-step function that will ensure that the Gaussian profile evolution ensues restrictively on the red side and Lorentzian profile of an unequal width shows up on the blue side of the spectrum profile-like scheme, and $k > 0$ (fundamental transition and overtones for $k = 1$ and $k \geq 2$, respectively) is the vibrational quantum number signifying the number of phonons associated with the vibronic transition. (FCFs have been precluded in Eq. 9 for clarity and simplicity.) For instance, in the case of one-phonon profile, $k = 1$

$$L_1 \propto \left[u(\omega - \omega_j) \frac{\gamma_j/2\pi}{(\omega - \omega_j)^2 + (\gamma_j/2)^2} + \frac{1}{\sqrt{2\pi\sigma_j^2}} u(\omega_j - \omega) e^{-(\omega - \omega_j)^2 / 2\sigma_j^2} \right] \quad (9a)$$

and $k = 2$ when it is a two-phonon profile (first overtone)

$$L_2 \propto \left[u(\omega - 2\omega_j) \frac{2\gamma_j/2\pi}{(\omega - 2\omega_j)^2 + (2\gamma_j/2)^2} + \frac{1}{\sqrt{2\pi\sigma_j^2}} u(2\omega_j - \omega) e^{-(\omega - 2\omega_j)^2 / 2\sigma_j^2} \right] \quad (9b)$$

γ_j denotes the width (full width at half maximum) of the Lorenzian profile associated with mode j, whereas σ_j is the corresponding standard deviation of the Gaussian distribution, yielding $fwhm = 2\sigma_j\sqrt{2\,ln\,2}$. In HSF, the one-phonon profile acts as the building block of the subsequent transitions (overtones) since they fold themselves with the one-phonon profile (fundamental transition), which will, in turn, build on the ZPL in the spirit of Born-Oppenheimer approximation. Henceforth, the subscript k will be dropped and j will denote vibrational mode j, and $R_{jnm}(t; \omega_j; \gamma_j)$ will be replaced with simply $R_{jnm}(t)$ to avoid clutter where confusion is unlikely to arise. L_1 in Eq. 9a is very similar to the spectral density reported by many groups (6,7,15–18,20–22,29).

Taking the inverse Fourier transform of L_1 of Eq. 9a yields the form of the nuclear dephasing function

$$R_{jnm}(t) = \mathcal{F}^{-1} \left[u(\omega - k\omega_j) \frac{k/2\pi}{(\omega - k\omega_j)^2 + (k\gamma_j/2)^2} + \frac{1}{\sqrt{2\pi\sigma_j^2}} u(k\omega_j - \omega) e^{-(\omega - k\omega_j)^2 / 2\sigma_j^2} \right]_{k=1} \quad (10)$$

Although the inverse Fourier transform of the first term (half-Lorentzian) in Eq. 10 is

$$\mathcal{L}_{jnm}(t) = \frac{1}{2\pi} e^{-i\omega_j t} \left\{ i e^{\gamma_j t/2} Ei\left(-\frac{\gamma_j}{2} t\right) + e^{-\gamma_j t/2} \left[\pi - i\,Ei\left(\frac{\gamma_j}{2} t\right) \right] \right\} \quad (11)$$

with Ei being the exponential integral function, the inverse Fourier transform of the second term (half-Gaussian) in Eq. 10 is

$$\mathcal{G}_{jnm}(t) = \frac{1}{2} e^{-i\omega_j t} e^{-\sigma_j^2 t^2 / 2} \left(1 + \mathcal{E}\mathrm{rf}\left(\frac{i\,\sigma_j\,t}{\sqrt{2}} \right) \right) \quad (12)$$

A word of caution about performing the integration in Eq. 10 that leads to the result in Eq. 11: the tabulated integrals and symbolic integration software produce a wrong result that excludes the $\pi\, e^{-\gamma_j t/2}$. The exponential integrals at $i\infty$ (complex infinity) that come up when evaluating Eq. 10 can be tricky, and therefore one has to exercise care while computing them, especially when $Ei(0) = -\infty$, $Ei(0) = \infty$, $Ei(i\infty) = i\pi$, and $Ei(0) = -\infty$; these values at infinity require adding a phase factor equal to π, which appears in Eq. 11. The tables of integrals shown in Ref. (30) seem to miss the factor π in Eq. 11. Multiple numerics have been performed to confirm this finding. Thus, the dephasing function $R_{jnm}(t)$ of the protein phonons for the vibrations reads

$$R_{jnm}(t) = \mathcal{L}_{jnm}(t) + \mathcal{G}_{jnm}(t) \quad (13)$$

$\mathcal{E}$ rf (.) in Eq. 12 is the error function typically found in Fourier analysis. Note that here the relationship $\sigma_j = \gamma_j/2\sqrt{2\,ln\,2}$ to link σ_j to γ_j, of which values may be chosen to fit experimental data, as reported in Ref. (15). Putting it together, Eq. 7 now reads

$$F_{jmn}(t) = exp\left[-i\varepsilon_{mn} t\delta_{mn} - iJ_{nm} t - S_{jnm}(1 - R_{jnm}(t)) - \Gamma_{ZPL}|t|/2 \right] \quad (14)$$

Eq. 14 gives the linear EDMCF that treats the electronic dephasing and phonon relaxation processes distinctively differently, unlike most mainstream

dephasing and relaxation models, including the MBO model. This feature alone makes this EDMCF unique, thereby making it superior to other models in that it is sensitive to both electronic dephasing and vibrational relaxation processes, thereby leading to asymmetric PSB in pigment-protein complexes (vide supra). (27) A word is in order concerning the dephasing function $\boldsymbol{R_{jnm}(t)}$ role, utility, and significance. The form of $\boldsymbol{L_1}$ of Eq. 9a draws on the findings of Small et al. (15–17,22) that the one-phonon profile could reasonably assume the form of Eq. 9a. However, it was never reported anywhere in this compact form as it appears in Eq. 9, especially introducing the unit step function, which is essential to assimilate the one-phonon profile correctly. The reason for calling $\boldsymbol{R_{jnm}(t)}$ a dephasing function is that it is the result of the inverse Fourier transform of a frequency-domain expression such as the one-phonon profile, which is essentially the spectral density of the bath phonons causing the dephasing and, hence, broadening. It is the spectral density from which the broadening effects emanate. As such, $\boldsymbol{R_{jnm}(t)}$ encodes the pigment-complex effect in that context in time domain; it is the counterpart of one-phonon profile in the frequency domain. For this reason, one-phonon profile plays a significant role in probing dephasing, hence the name. This explains why, when $\boldsymbol{R_{jnm}(t) = 0}$, we obtain an oscillatory function in Eqs. 7 and 14, exhibiting virtually no phonon damping activity. Thus, the utility of this dephasing function is to probe the asymmetry exhibited by the collective phonon motion experienced by the asymmetric distribution of phonons in the surrounding protein. This asymmetry of the phonon distribution manifests itself in homogeneous spectra in the PSB of condensed systems such as photosynthetic complexes.

The temperature dependence of the EDMCF may be obtained with the aid of lineshape function theory by utilizing (11,13,14)

$$\boldsymbol{F(t) = exp\left[- \int_{-\infty}^{\infty} \frac{1}{2\pi\omega^2}\left(\coth\left(\frac{\beta\hbar\omega}{2}\right)(1 - \cos(\omega t)) + i\sin(\omega t)\right) C(\omega)\, d\omega\right]}, \tag{15}$$

where $\boldsymbol{C(\omega)}$ is the bath spectral density. Thus, the final form of the optical EDMCF of mode j in the absence of population transfer reads

$$\boldsymbol{F_{jnm}(t) = exp\left\{ - i\varepsilon_{mn}t\delta_{mn} - iJ_{nm}t - \frac{\Gamma_{ZPL}|t|}{2} - \Xi_{jnm}\right\}} \tag{16}$$

where

$$\boldsymbol{\Xi_{jnm} = S_{jnm}\left\{ coth\left(\frac{\beta\hbar\omega_j}{2}\right)\left[1 - e^{i\omega_j t}\, R_{jnm}(t)\cos(\omega_j t)\right] + ie^{i\omega_j t} R_{jnm}(t) sin(\omega_j t)\right\}} \tag{16a}$$

Note that the ZPL profile is Lorentzian of width Γ_{ZPL} (full width, half maximum), whereas the multiphonon transitions making up the PSB of mode j would adopt half-Gaussian and half-Lorentzian distributions of widths equal to $\sigma_j\sqrt{k}$ on the low-energy side and $k\gamma_j$ on the high-energy side, respectively. Finally, one may obtain an expression of EDMCF for a multimode system with linear electron-phonon coupling whereby the PSB exhibits an asymmetric shape that may read

$$\boldsymbol{F_{jnm}(t) = exp\left\{ - \frac{\Gamma_{ZPL}|t|}{2} - \sum_{j=1}^{N}\left[i\varepsilon_{mn}t\,\delta_{mn} + iJ_{nm}t + \Xi_{jnm}\right]\right\}} \tag{17}$$

Eq. 17 represents the linear EDMCF of excitonically coupled paired pigments at finite temperatures for mode j and N-mode systems, assuming no population transfer. The unique aspect of Eq. 17 is fourfold: 1) it produces a homogeneous absorption spectrum that accounts for the asymmetry of the PSB and the symmetric shape of the ZPL; 2) it accounts for pigment-pigment coupling and for N-mode system correctly; 3) the one-phonon profile carries its width over the overtones through folding; 4) it avoids the N-convolutions that normally arise in the frequency domain, thereby speeding up the computation process significantly; and 5) it eliminates all the inconsistencies, deficiencies, and difficulties associated with the theory presented by HSF. It is also readily extendable to nonlinear spectroscopy, which will be presented in paper II.

Model and real system calculations

This section provides illustrative calculations for both model and real systems to ratify the above-derived EDMCF. Although the model calculation will employ average parameters of photosynthetic antenna pigment complexes where the pigment-pigment coupling is negligibly small and thus may be treated as a one-pigment system (6, 28, 19), the parameters of light-harvesting CP29 chlorophyll pigment-protein complex in green plants and the special pair reaction center in bacteria (pigment dimer) will represent system calculation. The adiabatic electronic energy gap $\Omega = 0$ throughout the course of calculations without loss of generality. For this reason, the ZPL,

fundamental transition, and overtones will be shifted by the interpigment coupling J, rendering the ZPL centered at J with $\Omega = 0$.

Fig. 1 uses model parameters $\Omega = J_{nm} = 0$, $S_j = 0.50$, $\omega_j \approx 30$ cm^{-1}, $\Gamma_{ZPL} = 1.0$ cm^{-1}, $\gamma_j = 20$ cm^{-1}, and $\sigma_j = 8.5$ cm^{-1} commonly found in monomeric pigment-protein complexes to calculate the linear homogenous absorption spectra at various temperatures. These parameters are judiciously chosen to explicitly display the structure brought about by taking

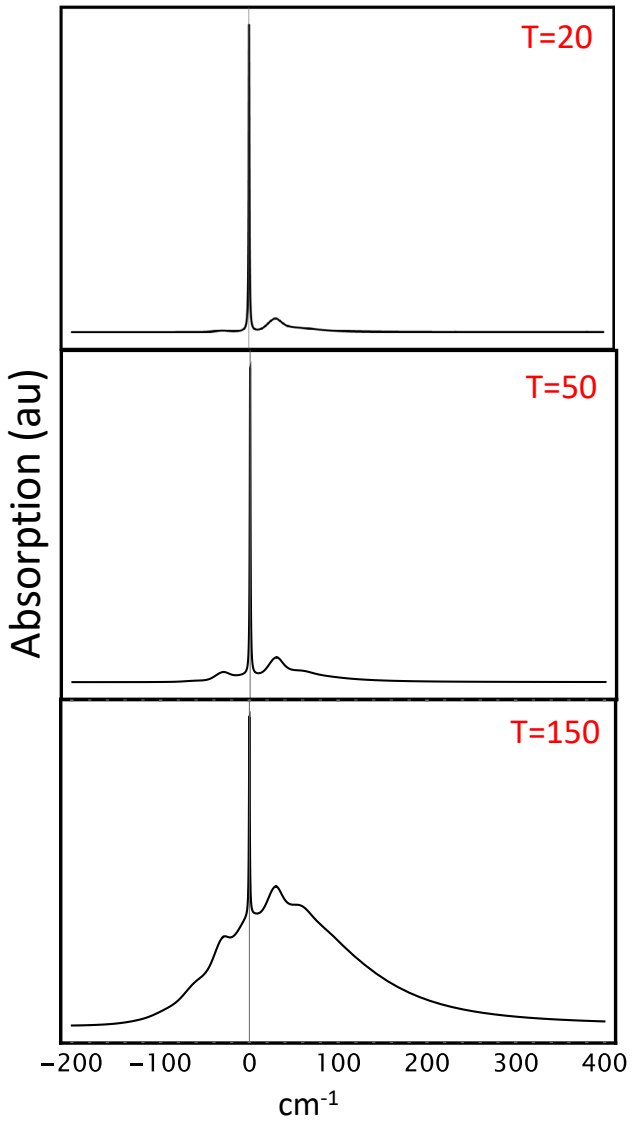

FIGURE 1 Linear homogenous absorption spectra at various temperatures, using the commonly found parameters in monomeric pigment-protein complexes with negligible excitonic coupling. $S_j = 0.50$, $\omega_j \approx 30$ cm^{-1}, $\Gamma_{ZPL} = 1.0$ cm^{-1}, $\gamma_j = 20$ cm^{-1} and $\sigma_j = 8.5$ cm^{-1}. All spectra show the ZPL as a sharp peak at $\omega = 0$ since the adiabatic electronic gap Ω was set to 0, $\Omega = 0$. The one-phonon profile is centered at $\omega = 30$ cm^{-1}, and hot bands arise as the temperature increases.

the Fourier transform of Eq. 17. All spectra show the ZPL as a sharp peak at $\omega = 0$ since the adiabatic electronic gap Ω was set to 0, $\Omega = 0$. One can also see the PSB, of which the one-phonon profile is the main component, on the blue side; such a weakly intense one-phonon profile centered at $\omega = 30$ cm^{-1} is an artifact of the weak exciton-phonon coupling $S_j = 0.50$, in line with the correct FCF of a linearly coupled system, as shown in the top panel at T = 50 K. As the temperature goes up, as shown in both the middle and bottom panels, although the ZPL intensity decreases, that of PSB becomes more intense with a hot band ($1 \leftarrow 0$ transition) peaked at $\omega = -30$ cm^{-1} on the red side. Further intensity loss of ZPL takes place as the temperature is elevated to T = 150 K, giving rise to a stronger PSB and more hot bands on the low-energy side. Fig. 2 calculates homogenous absorption spectra with linear exciton-phonon coupling (weak) at various temperatures. The absorption spectra in Fig. 2 utilize average parameters that are typically found in pigment-protein complexes, e.g., CP29 and B777: $S_j = 0.40$, $\omega_j \approx 30$ cm^{-1}, $\Gamma_{ZPL} = 1.0$ cm^{-1}, $\gamma_j = 60$ cm^{-1}, and $\sigma_j = 26$ cm^{-1}. The inset in the top panel cuts off the ZPL to better show the one-phonon profile. The inordinate ZPL strong intensity is attributed to the very weak exciton-phonon coupling ($S_j = 0.40$) and its narrow width. As the temperature goes up from T = 50 K to 250 K, more hot bands arise, giving more intensity to PSB. The inset in the top panel is shown after chopping off the sharp ZPL intensity to reveal the one-phonon profile better.

Finally, Fig. 3 uses the parameters of *Rps. viridis* BRC to calculate linear homogeneous spectra at different temperatures by Fourier transforming Eq. 17, where the mean frequency mode ($\omega_m = 30\ cm^{-1}$, $S_m = 2.1$, and $\gamma_m = 55\ cm^{-1}$) and the marker mode ($\omega_{sp} = 145\ cm^{-1}$, $S_{sp} = 1.0$, and $\gamma_{sp} = 50\ cm^{-1}$) are included with the width of $\Gamma_{ZPL} = 3\ cm^{-1}$ due to electronic decay, and the excitonic coupling $J_{nm} \sim 300\ cm^{-1}$. Fig. 3 reveals three linear homogeneous spectra *Rps. viridis* BRC calculated at various temperatures. The PSB predominates at T = 250 K, whereas the ZPL diminishes. The ZPL and phonon transitions (hot and cold) are shifted in all the spectra by $300\ cm^{-1}$ due to excitonic coupling.

Concluding remarks

The novelty of this work lies in not only presenting the electronic transition dipole moment correlation function in the time domain, which will allow an efficient and quick extension to finding nonlinear optical signals, but also using a G-L distribution function whereby both exciton-exciton coupling and exciton-phonon coupling are accounted for. This is an

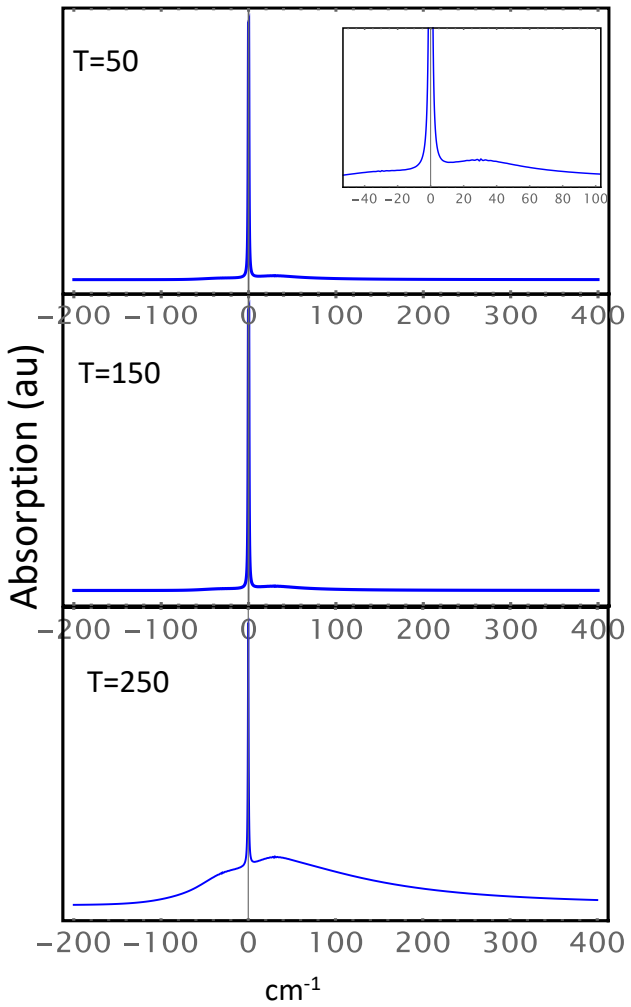

FIGURE 2 Linear homogenous absorption spectra at various temperatures. The spectra utilize the average parameters that are typically found in one-system pigments; e.g., CP29 and B777: $S_j = 0.40$, $\omega_j \approx 30$ cm^{-1}, $\Gamma_{ZPL} = 1.0$ cm^{-1}, $\gamma_j = 60$ cm^{-1}, and $\sigma_j = 26$ cm^{-1}. The inset in the top panel cuts off the ZPL to better show the one-phonon profile. The inordinate strong intensity of the ZPL is attributed to the very weak exciton-phonon coupling ($S_j = 0.40$) and its narrow width. As the temperature goes up, more hot bands arise, giving more intensity to the PSB. The inset in the top panel is shown after cutting off the sharp ZPL intensity to reveal the one-phonon profile better.

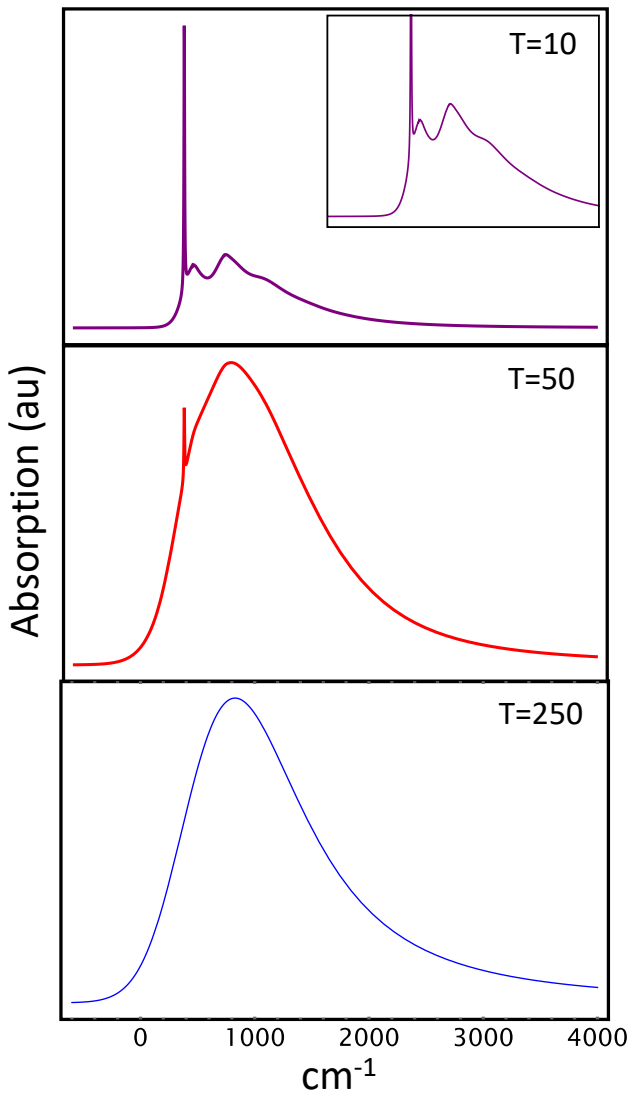

FIGURE 3 Linear homogeneous spectra of *Rps. viridis* BRC at different temperatures. Although the ZPL width is $\Gamma_{ZPL} = 3\,cm^{-1}$, due to electronic decay, the excitonic coupling $J_{nm} \sim 300\,cm^{-1}$. The parameters of the low-frequency mode are $\omega_m = 30\,cm^{-1}$, $S_m = 2.1$, and $\gamma_m = 55\,cm^{-1}$, whereas those of the marker mode are $\omega_{sp} = 145\,cm^{-1}$, $S_{sp} = 1.0$, and $\gamma_{sp} = 50\,cm^{-1}$. The PSB predominates at T = 250 K, whereas the ZPL diminishes. The ZPL and phonon transition (hot and cold) are shifted in all the spectra by 300 cm^{-1} due to excitonic coupling.

additional unique aspect of this work. As such, the focus of this article is to report and shed some light on the utility and correct applicability of G-L distribution function that experimentally seems to fit the one-phonon profile in some photosynthetic complexes in the time domain. One can, in turn, utilize the one-phonon profile structure to deduce the vibrational spectral density, which is a central quantity in probing energy transfer, rate constants of exciton transfer, exciton-phonon coupling strength, and lineshape calculations. The one-phonon profile is described using G-L distribution function with a coupling to a bath of low-frequency phonons governed by $g(\omega)D(\omega)$, where $g(\omega)$ is density of states and $D(\omega)$ is frequency-dependent coupling. The broadening, which is a consequence of the dynamical attributes of the molecules of the sample in question, and shape of the PSB reflect the nature of the constituent molecules making up the sample and its coupling to the surrounding environment. For this reason, this work may play biological role in ascertaining the nature of the phonon distribution embedded in the pigment-protein complexes,

thereby leading to a better understanding of the phonons making up the surrounding protein and vibrational structure of photosynthetic complexes, especially when probed using nonlinear spectroscopy techniques such as hole-burning, two-dimensional electronic spectra, and stimulated photon echo, all of which will be explored in the next series of this work in the future.

Although this work does not directly use the formulae of homogeneous absorption, hole-burning, and fluorescence line narrowing spectra of BRCs, and photosynthetic complexes, reported by Small et al. (15), it builds on their idea of the phonon sideband asymmetric shape in deriving an accurate and computationally efficient linear EDMCF that may readily be extended to derive and compute all nonlinear optical signals in frequency and time domains. Although paper II of this series will present illustrative nonlinear optical spectra of photosynthetic complexes and BRCs with asymmetric PSB, paper III will derive exact analytical expressions for the linear and nonlinear EDMCF and homogeneous spectra of the same system using lognormal distribution function (9,10,19) by using a newly developed spectral density called distorted Gaussian distribution that accounts for the PSB asymmetry, correct FCF, interpigment coupling, and electronic dephasing. The purpose of the distorted Gaussian distribution is to serve as an alternative to the lognormal spectral density that would circumvent the numerical challenges posed by lognormal distribution function.

AUTHOR CONTRIBUTIONS

All parts of this work were performed by M.T.

ACKNOWLEDGMENTS

This work was funded by UAE University Research Affairs under grant # G00003550.

DECLARATION OF INTERESTS

The authors declare no conflict of interest.

REFERENCES

1. Yang, S. J., E. A. Arsenault, …, G. R. Fleming. 2022. From antenna to reaction center: Pathways of ultrafast energy and charge transfer in photosystem II. *Proc. Natl. Acad. Sci. USA.* 119, e2208033119.
2. Arsenault, E. A., A. J. Schile, …, G. R. Fleming. 2021. Vibronic coupling in light-harvesting complex II revisited. *J. Chem. Phys.* 155, 096101.
3. Wang, L., M. A. Allodi, and G. S. Engel. 2019. Quantum coherences reveal excited-state dynamics in biophysical systems. *Nat. Rev. Chem.* 3:477–490.
4. Cao, J., R. J. Cogdell, …, D. Zigmantas. 2020. Quantum biology revisited. *Sci. Adv.* 6, eaaz4888.
5. Bose, A., and N. Makri. 2020. All-Mode Quantum–Classical Path Integral Simulation of Bacteriochlorophyll Dimer Exciton-Vibration Dynamics. *J. Phys. Chem. B.* 124:5028–5038.
6. Rätsep, M., R. Muru, and A. Freiberg. 2018. High temperature limit of photosynthetic excitons. *Nat. Commun.* 9:99.
7. Golub, M., L. Rusevich, …, J. Pieper. 2018. Rigid versus Flexible Protein Matrix: Light-Harvesting Complex II Exhibits a Temperature-Dependent Phonon Spectral Density. *J. Phys. Chem. B.* 122:7111–7121.
8. Jankowiak, R., M. Reppert, …, T. Reinot. 2011. Site Selective and Single Complex Laser-Based Spectroscopies: A Window on Excited State Electronic Structure, Excitation Energy Transfer, and Electron-Phonon Coupling of Selected Photosynthetic Complexes. *Chem. Rev.* 111:4546–4598.
9. Feng, X., A. Kell, …, R. Jankowiak. 2013. Modeling of the Optical Spectra of the Light-Harvesting CP29 Antenna Complex of Photosystem II – Part II. *J. Phys. Chem. B.* 117:6593–6602.
10. Reppert, M., A. Kell, …, R. Jankowiak. 2015. Comments on the optical lineshape function: Application to transient hole-burned spectra of bacterial reaction centers. *J. Chem. Phys.* 142, 094111.
11. Toutounji, M. 2009. Empirical relaxation function and spectral density for underdamped vibrations at low temperatures. *J. Chem. Phys.* 130, 094501.
12. Toutounji, M. M. 2003. The interplay between Matsubara terms and the contribution from the bath modes to the low-temperature zero-phonon line shapes for weakly damped modes. *Chem. Phys.* 293:311–321.
13. Mukamel, S., M. Toutounji, and G. J. Small. 1995. Principles Nonlinear Optical Spectroscopy, Oxford University Press: Oxford. *J. Chem. Phys.* 117:3848.
14. Toutounji, M., G. J. Small, and S. Mukamel. 1998. Optical response functions for condensed systems with linear and quadratic electron–vibration coupling. *J. Chem. Phys.* 109:7949–7960.
15. Hayes, J. M., P. A. Lyle, and G. J. Small. 1994. A Theory for the Temperature Dependence of Hole-Burned Spectra. *J. Phys. Chem.* 98:7337–7341.
16. Lyle, P. A., S. V. Kolaczkowski, and G. J. Small. 1993. Photochemical Hole-Burned Spectra of Protonated and Deuterated Reaction Centers of Rhodobacter sphaeroides. *J. Phys. Chem.* 97:6924–6933.
17. Reddy, N. R. S., S. V. Kolaczkowski, and G. J. Small. 1993. Nonphotochemical Hole Burning of the Reaction Center of Rhodopseudomonas viridis. *J. Phys. Chem.* 97:6934–6940.
18. Pieper, J., P. Artene, …, A. Freiberg. 2018. Evaluation of electron–phonon coupling and spectral densities of pigment–protein complexes by line-narrowed optical spectroscopy. *J. Phys. Chem. B.* 122:9289–9301.
19. Adam, K., R. E. Blankenship, and R. Jankowiak. 2016. Effect of Spectral Density Shapes on the Excitonic Structure and Dynamics of the Fenna–Matthews–Olson Trimer from Chlorobaculum tepidum. *J. Phys. Chem. A.* 120, 36146.
20. Pieper, J., J. Voigt, …, G. Small. 1999. Analysis of phonon structure in line-narrowed optical spectra. *Chem. Phys. Lett.* 310:296–302.
21. Pieper, J., M. Rätsep, …, G. J. Small. 1999. Q_y-Level Structure and Dynamics of Solubilized Light-Harvesting Complex II of Green Plants: Pressure and Hole Burning Studies. *J. Phys. Chem. A.* 103:2412–2421.
22. Reddy, N. R., P. A. Lyle, and G. J. Small. 1992. Applications of spectral hole burning spectroscopies to antenna and reaction center complexes. *Photosynth. Res.* 31:167–194.

23. Lin, C., M. Reppert, …, R. Jankowiak. 2014. Modeling of fluorescence line-narrowed spectra in weakly coupled dimers in the presence of excitation energy transfer. *J. Chem. Phys.* 141, 035101.

24. Toutounji, M. 2021. Electronic dephasing of polyatomic molecules interacting with mixed quantum-classical media. *Phys. Chem. Chem. Phys.* 23:21981–21994.

25. Toutounji, M. 2022. Electronic dephasing in mixed quantum–classical molecular systems using the spin-boson model. *Physica A.* 585, 126385.

26. Knox, R. S., G. J. Small, and S. Mukamel. 2002. Low-temperature zero phonon lineshapes with various Brownian oscillator spectral densities. *Chem. Phys.* 281:1–10.

27. Arfken, G. 1985. Mathematical Methods for Physicists. Academic Press.

28. Kell, A., X. Feng, …, R. Jankowiak. 2013. On the Shape of the Phonon Spectral Density in Photosynthetic Complexes. *J. Phys. Chem. B.* 117:7317–7323.

29. Rätsep, M., J. Pieper, …, A. Freiberg. 2008. Excitation Wavelength-Dependent Electron– Phonon and Electron– Vibrational Coupling in the CP29 Antenna Complex of Green Plants. *J. Phys. Chem. B.* 112:110–118.

30. Gradsteyn, I. S., and I. M. Ryzhik. 2007. Tables of Integrals, Series and Products. Academic Press, New York.